



IAC SUMMER FELLOWSHIP IN ASTRONOMICAL RESEARCH 2022

On the origin of M87's globular clusters

Kiara Hervella Seoane

Project's PI: Almudena Prieto Escudero

2022

A.1 Resumen

Se han analizado imágenes de alta resolución espacial de M87 en el rango óptico e infrarrojo, de NaCO-VLT y HST, para derivar el perfil de brillo superficial de M87 en la región central de $80''$. Utilizando resultados previos de la literatura, obtenidos a partir de observaciones en IR en los $19.2''$ centrales y en el rango óptico para los $80''$, hemos clasificado estos GC en las dos principales subpoblaciones: cúmulos rojos o ricos en metales y azules o de baja metalicidad. Estas subpoblaciones coinciden con la clásica bimodalidad de las distribuciones color para los cúmulos globulares de galaxias gigantes elípticas. Hemos calculado los perfiles de densidad superficial para las dos subpoblaciones de GC, observadas en el infrarrojo, en la región más interna de $19.2''$. Su concordancia con el perfil obtenido a partir de las observaciones ópticas, hasta $80''$, indica la ausencia de extinción en las detecciones debida al polvo.

Para los GC detectados en el rango óptico, los GC rojos dominan el perfil de densidad superficial en toda la región estudiada. Desde una distancia radial de $35''$ en adelante, los perfiles de densidad superficial de los GC rojos y azules coinciden con el perfil de brillo superficial de M87. Dentro de esta distancia, la densidad de GC azules disminuye hacia el centro hasta casi desaparecer. La distribución de los GC rojos sigue el mismo comportamiento que el M87 hasta $20''$ (1.5 kpc), donde su distribución se vuelve más plana que el perfil de brillo de M87. Estos resultados, junto con los resultados de otros autores (la similitud en color entre M87 y los GC rojos, así como su distribución centralmente concentrada) podrían respaldar tentativamente el escenario en el que los GC rojos comparten formación común con M87, mientras que los GC azules se habrían acretado debido a canibalización de otras galaxias (mostrando un perfil de densidad superficial más extenso y siendo pobres en metales). La falta del GCS esperado dentro de unos pocos kpc del centro galáctico habría sido consumida por el agujero negro central.

A.2 Abstract

High spatial resolutions images of M87 in the optical and infrared range, from NaCO-VLT and HST, have been analysed for deriving the stellar surface brightness profile of M87 in the most central region, under $80''$. Using literature previous results, from IR observations in the inner $19.2''$ and in the optical range for the inner $80''$, we classified the detected GCs in these regions into the two main metal-rich red and metal-poor blue GCs subpopulations, associated with the typically found GCs colour distribution bimodality in giant ellipticals. We have computed the surface density profiles for the two GCs subpopulations, observed in the infrared, in the innermost region of $19.2''$. Its agreement with the profiles derived from optical observations, till $80''$, show no dust extinction affecting the GCs detection.

For the GCs detected in the optical range, red GCs dominate the surface density profile in the whole studied region. From a radial distance of $35''$ on, both red and blue GCs surface density profiles agree with M87 surface brightness profile. Inside this distance, the density of blue GCs decreases towards the center till almost fading. Red GCs distribution follow the same behaviour as M87 till $20''$ (1.5 kpc), were their distribution becomes flatter than M87 light profile. These results, along with other authors' results (the similar colour between M87 and the red GCs and its centrally concentrated distribution) could tentatively support the scenario where red GCs share a common formation scenario with M87, while blue GCs would have been accreted due to canibalization of other galaxies (showing a more extended surface density profile and being metal-poor). The lack of expected GCS within a few kpc of the galactic centre would then have been accreted by the central black hole.

Contents

B Background and current state of the topic	1
B.1 Metallicity in globular clusters	1
C Hypothesis and objectives	2
D Material and methods	3
D.1 Data	3
D.1.1 Infrared images	3
D.1.2 Globular clusters	3
D.2 Methodology	5
D.2.1 Extraction of the surface brightness profile	5
D.2.2 Extrapolation of the surface brightness profile	7
D.2.3 Computation of the globular clusters subpopulations and radial distribution	10
E Results and discussion	13
E.1 Surface brightness profiles	13
E.1.1 Globular cluster radial distribution	14
F Conclusions	17

B Background and current state of the topic

M87 is a giant elliptical galaxy at the center of the Virgo galaxy cluster. This type of giant ellipticals are commonly known as brightest cluster galaxies (BCGs), and they are key systems in performing stringent tests for proving and verifying the current theories of galaxy formation. Multiple models of galaxy formation for this brightest cluster galaxies predict dualistic star formation histories, where most of the stellar mass is formed very early, while the rest of mass is assembled later on, due to the merging of smaller galaxies that are also and already old (De Lucia & Blaizot 2007). So the multiple field star populations differ in their metallicity, but do present similar ages.

At the same time, it is thought that the globular clusters (GCs) within this BCGs are formed during the major episodes of the field star formation, containing then information about the formation and evolution of their host galaxy. Multiple deep imaging studies performed in BGCs have revealed systems of globular clusters with bimodal optical colour distributions (Kundu et al. 1999; Peng et al. 2006), attributable to different episodes of star formation. As in field stars populations, since all GCs are uniformly old, their colour bimodality is due principally to a metallicity difference between the two subpopulations. The bluer GCs colour and spatial distributions are consistent with those of the metal-poor halo stars in our host Galaxy, while red GCs have optical colours and spatial distributions similar to the ones in the bulge of their host galaxies (Kundu et al. 1999; Peng et al. 2006). Besides that, the mean metallicity of the metal-rich GCs correlates well with parent galaxy luminosity, which indicates that the metal-rich GCs are closely coupled to the galaxy and share a common chemical enrichment history with the galaxy field stars (Forbes et al. 1997). Therefore, the bluer CGs in BCGs can be considered as accreted by the host galaxy from the surroundings, originally formed in low-mass matter haloes in the early Universe, and assembled to the galaxy. While, the metal-rich red GCs would be borned in the subsequent buildup of the parent galaxy, getting physically associated with the stellar body. Detailed studies of the GCs subpopulations can then offer some constraints on hierarchical galaxy formation.

The unusually rich system of globular clusters around the giant elliptical galaxy M87, along with its simple morphology and proximity, presents an excellent opportunity to study the structural relationship between globular cluster systems and their parent galaxies. The number density distribution of GCs with radius allows us to investigate the spatial distribution of GCs and to trace the original distribution of matter within the host galaxy, since they are the oldest known systems in the Universe. Previous studies have derived surface density profiles for the GC system and its separate subpopulations in M87 (Forbes et al. 2004; Harris 2009; Lauer & Kormendy 1986; Strader et al. 2011). By studying ≈ 750 GCs, Strader et al. (2011) found that the radial distribution of the blue GCs is more extended at larger radius, while the red GCs are more centrally concentrated and their radial profile resembles the light profile of field stars of the galaxy up to $30'$. Another striking difference between both these subpopulations is that the mean colour of the red GCs correlates with the luminosity of the host galaxy (Forbes et al. 1997; Larsen et al. 2001). Both these features suggest a common formation scenario for both systems.

B.1 Metallicity in globular clusters

A way to estimate the metallicity of a stellar population, is using its V - I colours. Models have shown that beyond a few Gyr, the colour of a star cluster is predominantly determined by its metal content (Bruzual & Charlot 2003; Vazdekis et al. 2012). There are experimental relationships that rely on parametrizations of this link between colour and metallicity. They used spectroscopic derived metallicities and integrated colours for Milky Way GCs (Harris et al. 2000) but in recent works it has been extended to extragalactic GCs (Peng et al. 2006; Sohn et al. 2006). Using also M87 globular clusters, Sohn et al. (2006) derives a linear colour-metallicity relationship. Even though that their modelled transformations present scatter in the data, the colour-metallicity relationship seems tight enough to derive such fit.

Since GCs are old but simple stellar populations, broadband colours should be a good approximation for metallicity, but it must be taken into account that the main limitation of this approach is the poorer sensitivity of the optical colours to metallicity.

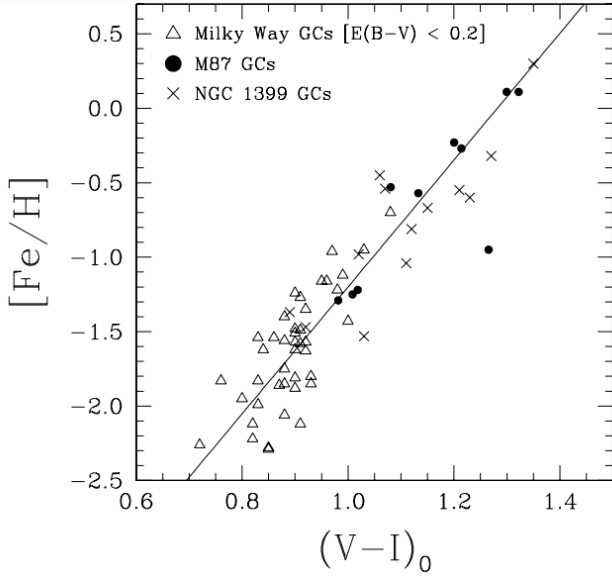


Figure 1: Correlation between $(V-I)_0$ color and $[\text{Fe}/\text{H}]$ for Milky Way GCs with $E(B-V) < 0.2$ (triangles), M87 clusters (circles), and NGC 1399 clusters (crosses). The solid line is a result of fitting the data points with the bisector method. Image taken from Sohn et al. (2006).

C Hypothesis and objectives

Using observations of high spatial resolutions in the optical and infrared range, we can derive the stellar surface brightness profile of M87, produced mainly by the old star populations that conform this galaxy, till the galactic centre. This profile can be considered as a simple but concrete estimate of the original matter distribution of hot cosmological haloes, from which the whole M87 galaxy and its central black hole have been formed.

By comparing the surface brightness profile in the most central region with the radial numerical distribution of each globular cluster subpopulation, considered as the older systems in the Universe, we can study the formation relation between the whole galaxy and its field stars and the globular clusters subpopulations. The comparison between both these distributions, the old stellar population and the red and blue old globular clusters, will provide us information about the origin and formation region of the globular clusters subpopulations within the host galaxy. If the profiles are coincident, globular clusters would have been formed inside the galaxy (or outside if they are divergent). If our work supports the scenario where red globular clusters are formed within the galaxy, this result would have a fundamental impact on the theories about the origin of M87-like galaxies and their formation from cosmological haloes.

The main objective of this project is to familiarise with the M87 galaxy and its central black hole, while visualizing and studying optical and infrared images of its galactic centre. The surface brightness profile of the galactic centre of M87 must be extracted around the central kpc, and compared with the globular cluster radial distribution for each subpopulation within the same region. The comparison between both these profiles will allow us to infer about the origin of the globular clusters and M87 itself.

D Material and methods

D.1 Data

In order to achieve the main goal of this project, we need to choose images of high-spatial resolution that allow us to derive the stellar surface brightness profile and to locate the position of the different globular clusters within the galaxy in the most central region. Since our interest in the surface brightness profile is to trace the old field stellar populations within the M87 galaxy, consequently we decided to retrieve images, previously used by other authors, in the infrared range. For the globular clusters distribution. we have benefited from the photometry and localization results by Montes (2013) and by Bellini et al. (2015).

Besides all of this, the distance we have adopted for M87 is 16.1 Mpc, which is consistent with analyses of surface brightness fluctuations (Blakeslee et al. 2001). Even though that in terms of surface brightness distribution the effective radius and luminosity of M87 are highly uncertain (and perhaps even ill-posed quantities), we have chosen as reference the results from Kormendy et al. (2009): $R_e = 3.2$ (16 kpc) and $M_v = -22.86$.

D.1.1 Infrared images

The infrared data used in this project are three high-spatial resolution images (that can be seen in Figure A in the Appendix). One of the images was observed with the NaCO instrument, mounted at one of the 8.2m diameter telescopes of the Very Large Telescope (VLT), located in Cerro Paranal (Chile). NaCO stands for Nasmyth Adaptive Optics System (NAOS) plus the NearInfrared Imager and Spectrograph (CONICA), providing AO assisted imaging with several cameras that allow diffraction limited sampling. The image was taken in 2005-01-20 using the infrared K-band filter, centered at $2.2 \mu m$. NaCO presents a really high spatial resolution with a plate scale value of $0.0271''$ per pixel and a field of view of $22 \times 22''$ (which implies a radial distance from the centered M87 of $\approx 11''$, while the spatial resolution¹ due to the seeing of this observation was of $\theta(\text{FWHM}) \approx 6 \text{ pixels} = 0.16''$.

The other image was observed using the ultraviolet and visible light (UVIS) channel of the Wide Field Camera 3 (WFC3), installed at the 2.4m diameter Hubble Space Telescope (HST). The data was observed on 2016-01-24 in the F814W filter, centered around $8140 \text{ \AA} = 0.814 \mu m$, similar to the SDSS near infrared I band. The WFC3/UVIS channel presents a plate scale of $0.04''$ per pixel, but the spatial resolution of this concrete observation was $\theta(\text{FWHM}) \approx 3 \text{ pixels} = 0.12''$. The field of view in this case is of $43.64 \times 41.44''$ (without taking into account the bad pixels in the outer regions due to the parallelogram shape of the CCD image).

The third image was observed with the Wide Field Channel (WFC) channel of the Advanced Camera for Surveys (ACS), installed also at the Hubble Space Telescope (HST). The data was observed on 2003-01-19, using the infrared F850LP filter, centered around $8140 \text{ \AA} = 0.967 \mu m$, like the SDSS Z band. The ACS WFC channel presents a plate scale of $0.05''$ per pixel, and the spatial resolution of the image was $\theta(\text{FWHM}) \approx 3 \text{ pixels} = 0.15''$. Without taking into account the bad pixels due to the parallelogram distribution of the HST images, the wide field of view of the image is of around $3.5 \times 3.5'$.

D.1.2 Globular clusters

For studying the distribution of the globular clusters we have chosen the already derived results from Montes (2013) and from Bellini et al. (2015).

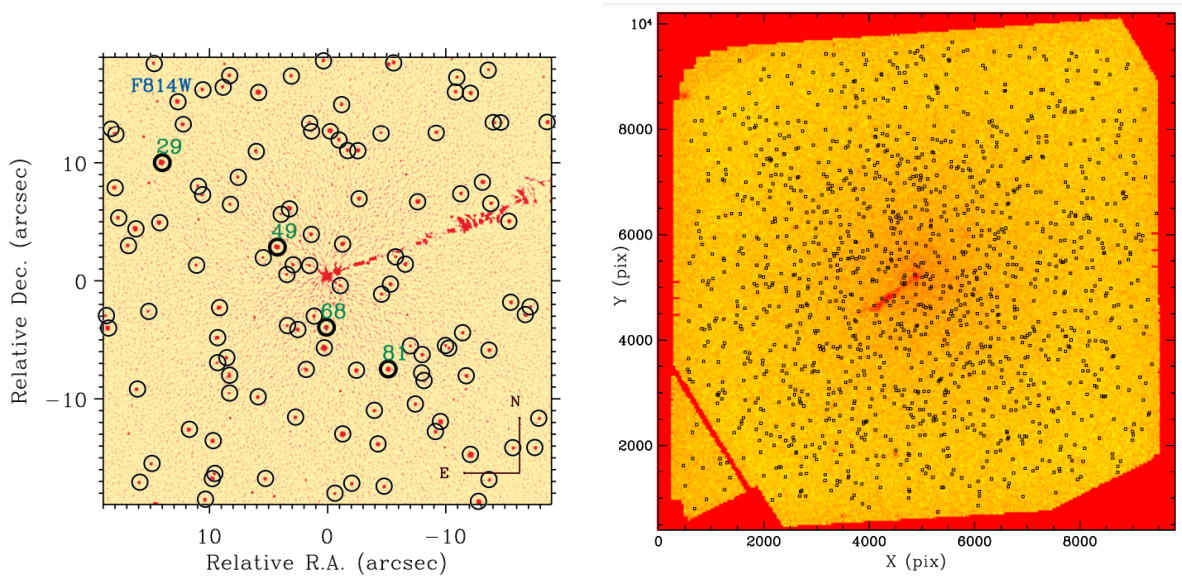
Montes (2013), within the PARSEC project, has derived the positions and photometry of 115 globular clusters² in the central $38.4 \times 38.4''$ ($\approx 3 \times 3 \text{ kpc}^2$), relative to the center of M87. The high density of stars, internal reddening and existent AGNs in the centre of galaxies make the central region a difficult environment to detect fainter objects such as GCs. Specially, for early-type galaxies such as M87, the underlying massive host galaxy outshines the light of these systems for central locations, making it hard to decouple the brightness profiles of the host galaxy from those of the sources near the centre of the galaxy. So, once again, high-resolution AO imaging

¹The spatial resolutions of the observed images were studied using the task *imexam* from IRAF

²The lists of detected sources can be seen in Table A.1. of Montes (2013).

was the more appropriate approach for studying these areas. Montes (2013) used a data sample of NIR J-band and K_s -band images observed also with NaCO³, and UV-optical images from the HST archival data. Then, they used the unsharp-masking method (Sofue, 1993) to enhance the contrast and facilitate the detection of the GCs, and then the diffuse galaxy light was subtracted from the original image to facilitate detection. The lists of detected sources in each image were cross-correlated to create the final catalogue available in their paper, that provides us their right ascension and declination relative to the nucleus. In addition, using HST-ACS images, the photometry was performed for the F606W and F814W filters and transformed into Vega magnitudes for the standard V and I broad band filters, respectively. The results can be easily used for classify the GCs into the two known subpopulation and to generate their radial numerical density distribution in the most inner region.

1460 globular clusters in the central $2.7 \times 2.7'$ were found and studied by Bellini et al. (2015), using images of multiple exposures from the HST (WFC3/UVIS and ACS), in the optical-UV range. The sources were detected using the publicly available FORTRAN program *imag2xym_WFC.09X10*, that employs “library” effective PSFs that vary spatially across the detector and permit to detect and perform the photometry of the GCs. The photometry was performed for the F606W and F814W HST filters, that can be considered as an approximation of the V and the I Sloan broad bands. These results would also allow us to generate the radial numerical density distribution of the different globular cluster subpopulations but to a greater distance from the centre of M87, while maintaining the high spatial resolution. More extended profiles would help us in the comparison with previous results from the literature.



(a) Montes (2013) masked HST-ACS F814W-band image of the central $20''$ of M87. The 115 GCs identified are encircled. Image taken from Montes (2013).

(b) Montes (2013) HST-ACS F814W-band map of the central $2.7'$ ($\approx 3 \times 3 \text{ kpc}^2$) of M87. The 1460 GCs identified are encircled. Image taken from Bellini et al. (2015).

Figure 2: Globular clusters samples

³More information about the images and its spatial resolution can be seen in the Section 3 from Montes (2013)

D.2 Methodology

D.2.1 Extraction of the surface brightness profile

The high resolution surface brightness profiles of M87, obtained from the previously presented images, were derived using the task *ellipse* from IRAF. *ellipse* searches for the best-fitting isophotes by iteratively sampling the image along elliptical paths with a given semimajor axis length.

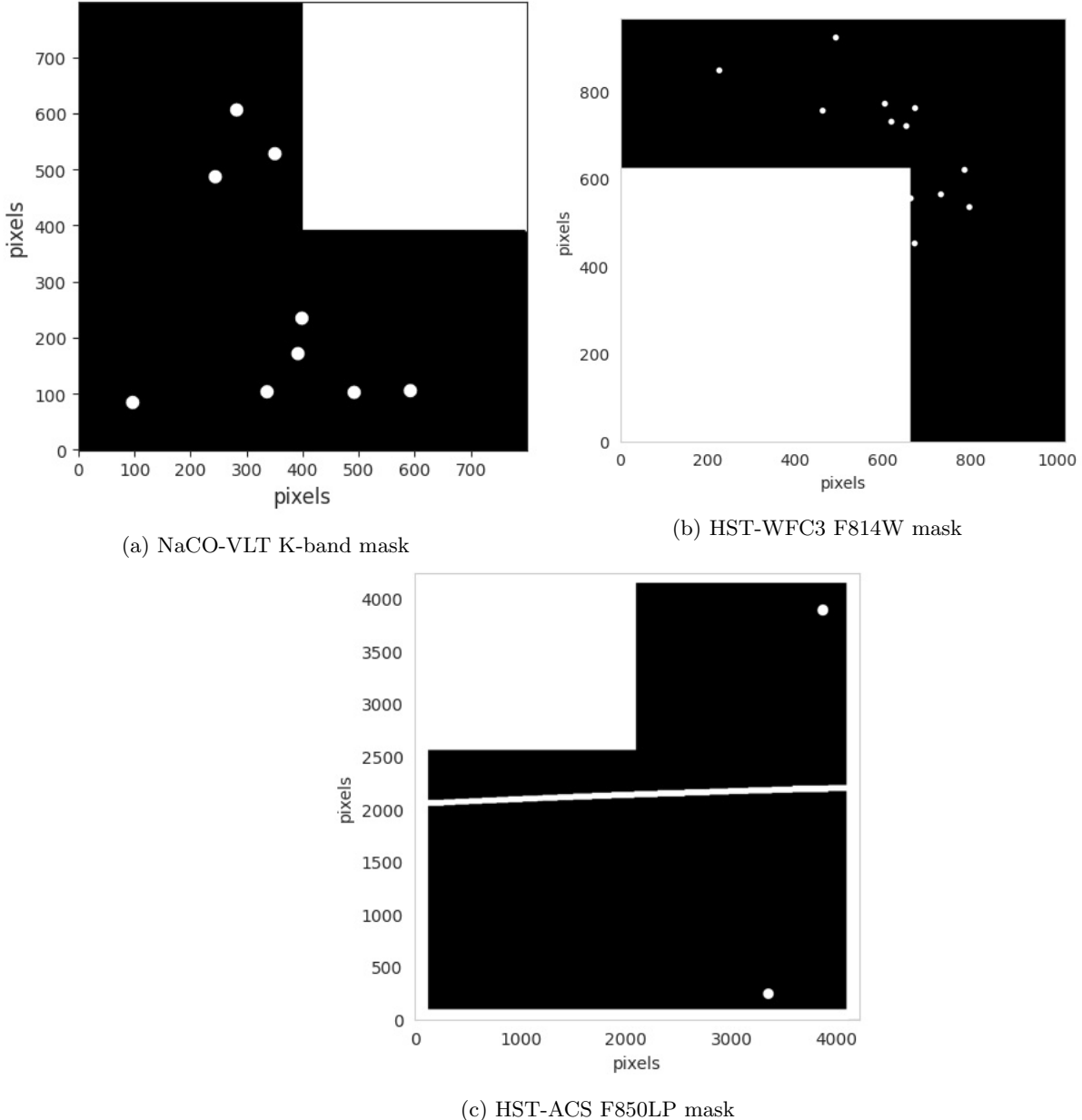


Figure 3: CCD masks used for deriving the surface brightness profile with the IRAF task *ellipse*.

After performing a few running tests, we concluded that there was a need for identifying and masking the prominent jet of M87, due to its strong effect in the surface brightness profile of the galaxy, specially in the case of the NaCO K-band image. The NaCO K-band image that was observed in 2005, during a powerful outburst (that lasted from 2003 to 2007), were the jet and its first knot became extremely luminous (López-Navas & Prieto 2018). Since M87 emission is circular symmetric (Cohen et al. 1998), we computed masks where the quadrant affected by the jet was completely masked in all images⁴, as can be seen in the mask images presented in Figures 2. The most luminous globular clusters detected were also masked for each image, using the task *imedit* from IRAF. In order to completely get rid of these globular clusters emission, by centering in the centre of each GC, 2 times the FWHM/seeing of each observation was masked (12 pixels = 0.325 " for the NaCO-VLT K-band image and 6 pixels = 0.24 " for the HST-WFC3 F814W image). These values were chosen based on the fact that due to the high spatial resolution of these images, the secondary lobes of the PSF for luminous objects could still be very dominant. For the wide HST-ACS F850LP CCD image, some luminous objects within the same field of view were masked, instead of the GCs, using apertures big enough for masking all their emission.

The images (Appendix, Figure A)and the created masks⁵ were then provided to the IRAF *ellipse* task in order to derive the surface brightness profiles. For both images, the center position of M87, a small ellipticity value of 0.1 and the observed position angle were provided as initial guesses. The control parameters were unconstrained, so the center, ellipticity and position angle were allowed to vary independently for each fitted isophote, but some limit values were imposed for the regions. For the large HST-ACS F850LP image, we studied a region of just 85 " around the position of M87, rather than the whole field of view, since it was necessary to compromise between keeping good non-noisy results and obtaining a range enough to compare with the GCs distribution (the Bellini data goes till a radial distance of $1.35' \approx 80''$). The semimajor axis step given for sampling the ellipses around the galaxy was of 1 pixel, for reproducing all the available flux information, searching for the highest possible resolution for these images (without oversampling them).

We must mention that while fitting with *ellipse*, the function stops at 3 pixels from the center of the galaxy ($0.08'' = 6$ pc in NaCO, $0.12'' = 9$ pc in the HST-WFC3 image and $0.15'' = 0.12$ pc for HST-ACS) due to the statistical lack of points for performing the fit, so this computational limit has determined how close our results can get to the exact centre of M87. At the same time, we have also imposed that the elliptical sampling must be forced to stop when the percentage of flagged (deviant or previously masked) points within the same elliptical path is greater than the 50%. This criteria has stopped the extracted profiles a few pixels before the actual limit of the images, were the background noise within the image is a little bit larger and significant and were there is not enough available data outside the limits of the field.

The *ellipse* task mainly outputs of our interest are the intensity of the isophotes and its correspondent semimajor axis length, in the same instrumental units as the provided CCD image (ADU/s and pixels, respectively). These information was transformed to meaningful physical units. In the case of the semimajor axis length, the plate scale of each image had to be taken into account. For the intensity values, they were transformed into $\text{mag}/''^2$, since they were representing a surface brightness profile⁶:

$$m[\text{mag}/''^2] = m_0[\text{mag}] - 2.5\log_{10}\left(\frac{I[\text{ADU}/\text{s}] \cdot \text{sens}[\text{erg}/\text{cm}^2/\text{A}/\text{ADU}]}{\text{scale}^2[''/\text{pixel}]}\right) \quad (1)$$

The resulting surface brightness profiles can be seen in Figure 3.

As a way to verify each of the extracted surface brightness profiles, we have used them to generate 2D models of M87 in order to subtract them from the original images and examine the resulting residuals. For generating the galaxy model, the IRAF task *bmodel* was used. This task uses the information available in the output tables obtained from *ellipse* to reconstruct the extracted elliptical isophotes: intensity of the isophote, semimajor axis length, center, ellipticity and position angle. The models and residual images can be seen in Figures 4 and 5.

⁴Must be clarified that masking the quarter part of M87 does not imply any information losses due to its mentioned symmetry.

⁵The mask provided to the IRAF *ellipse* task must be in a .pl format.

⁶All the sensitivity and zeropoint (m_0) values are easily accessible in the header of each studied image.

D.2.2 Extrapolation of the surface brightness profile

The extracted surface brightness profiles reach the most nuclear region of M87 (3 pixels away from its centre), so the contribution of its nuclei is visible in the profiles as the central steep spike (Figure 3 and Figure 4). Since our surface brightness profiles are meant to study the old field stars light distribution they must be representative of the bulge of M87. This is the reason behind the need of subtracting the nuclear contribution.

The nucleus of M87 is actually a point source, but it appears extended due to the PSF of each observation, that can be characterized by its FWHM value ($\theta(\text{FWHM}) \approx 6 \text{ pixels} = 0.16''$ for VLT-NACO, $\theta\text{L.}(\text{FWHM}) \approx 3 \text{ pixels} = 0.12''$ for HST-WFC3 and $\theta(\text{FWHM}) \approx 3 \text{ pixels} = 0.15''$ for HST-ACS). It would be expected that the contribution of the nuclei would not surpass a extension of around $3 \cdot \theta(\text{FWHM})$, associated with the main lobe of the PSF and its wings. But, since the PSF distribution is actually weighted by the luminosity of the point source, the secondary lobes (or Airy diffraction rings) are contributing to the surface brightness profile and are actually observable in some cases. Specially, in the NaCO image (Figure 6), which present the greater spatial resolution, some structure in the most central region (inside $1.36''$) can be seen that could be an effect off the Airy disc distribution from the nuclei emission. This contribution can even dominate the rest of emission since M87 nuclei is very powerful and luminous.

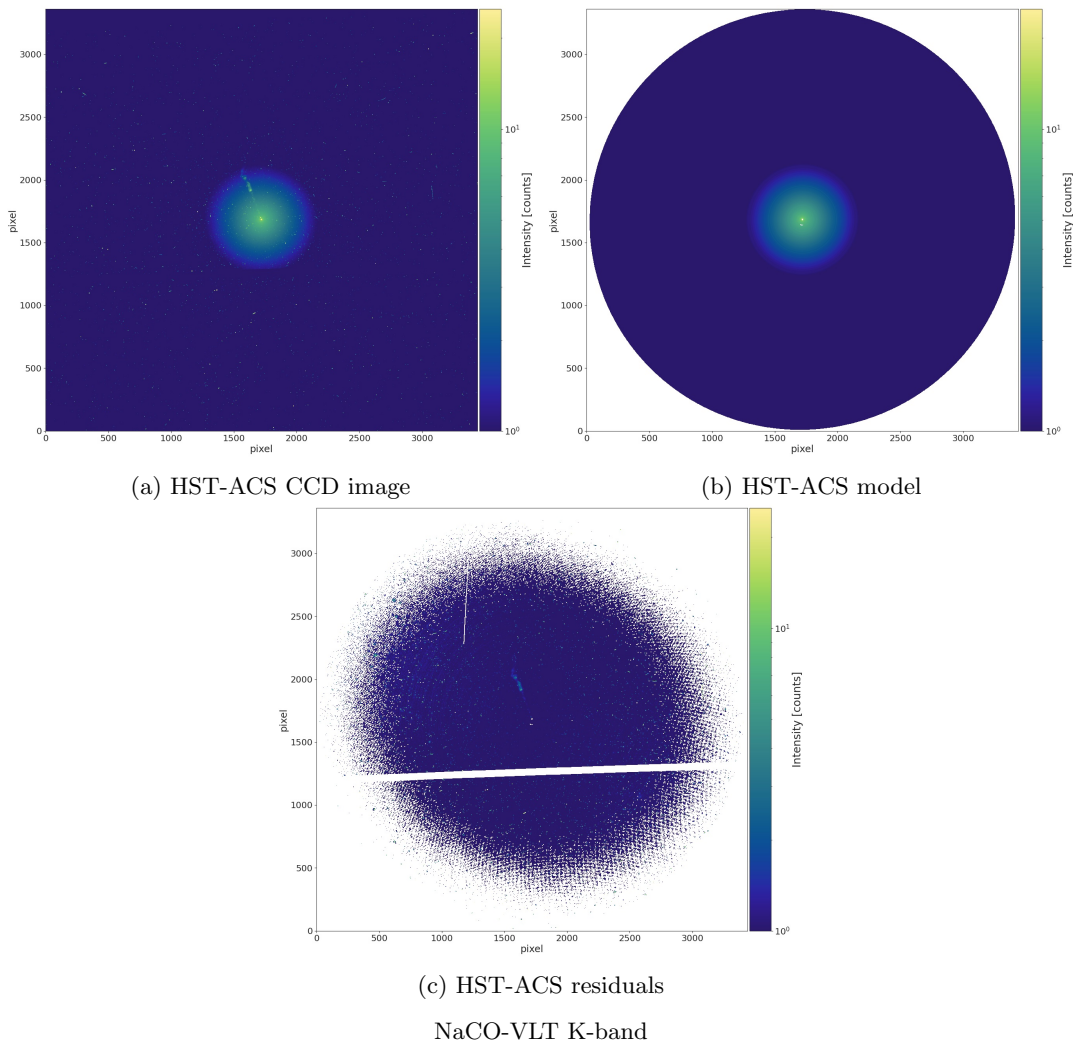


Figure 4: CCD image, model and residuals obtained for the HST-ACS image.

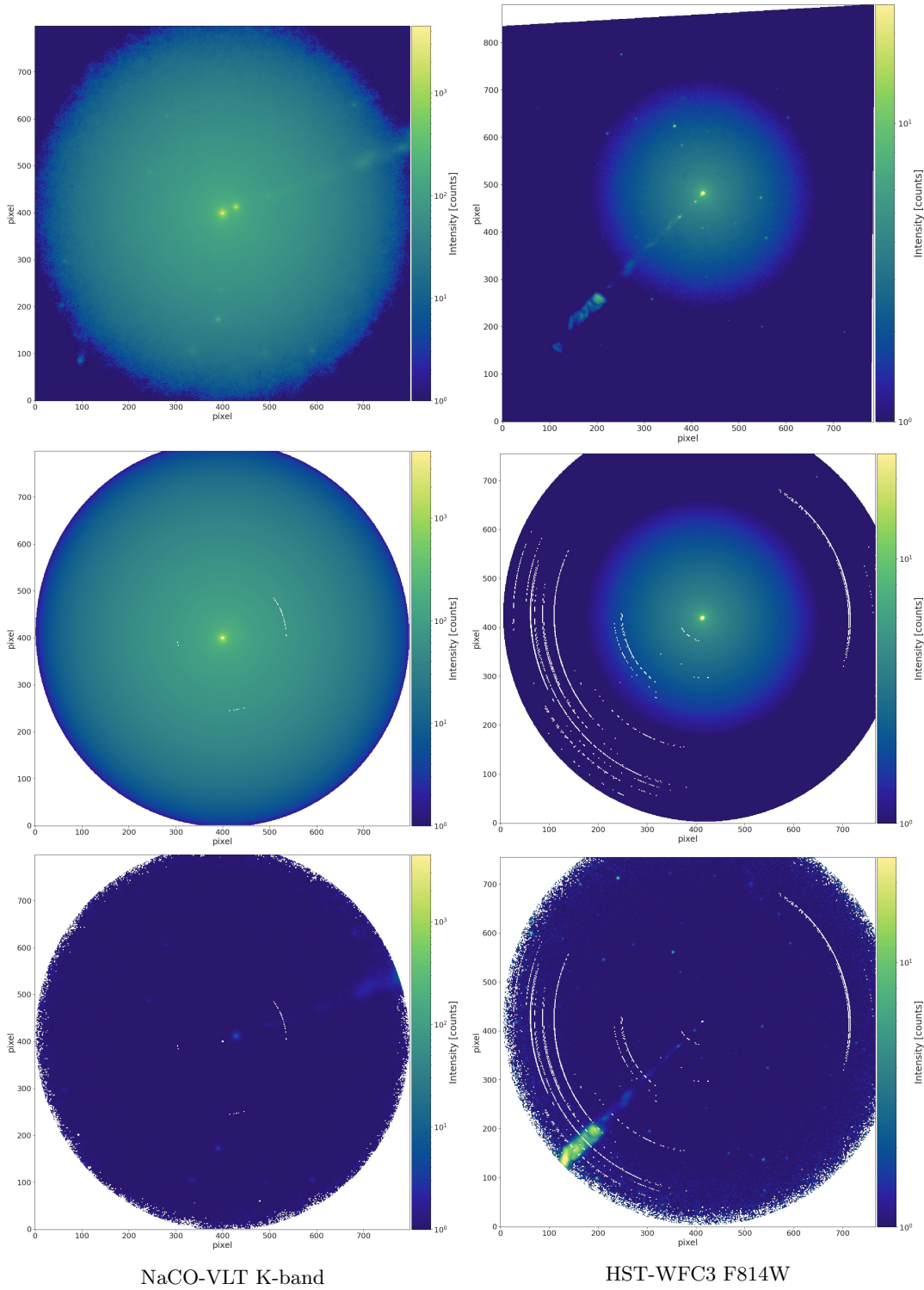
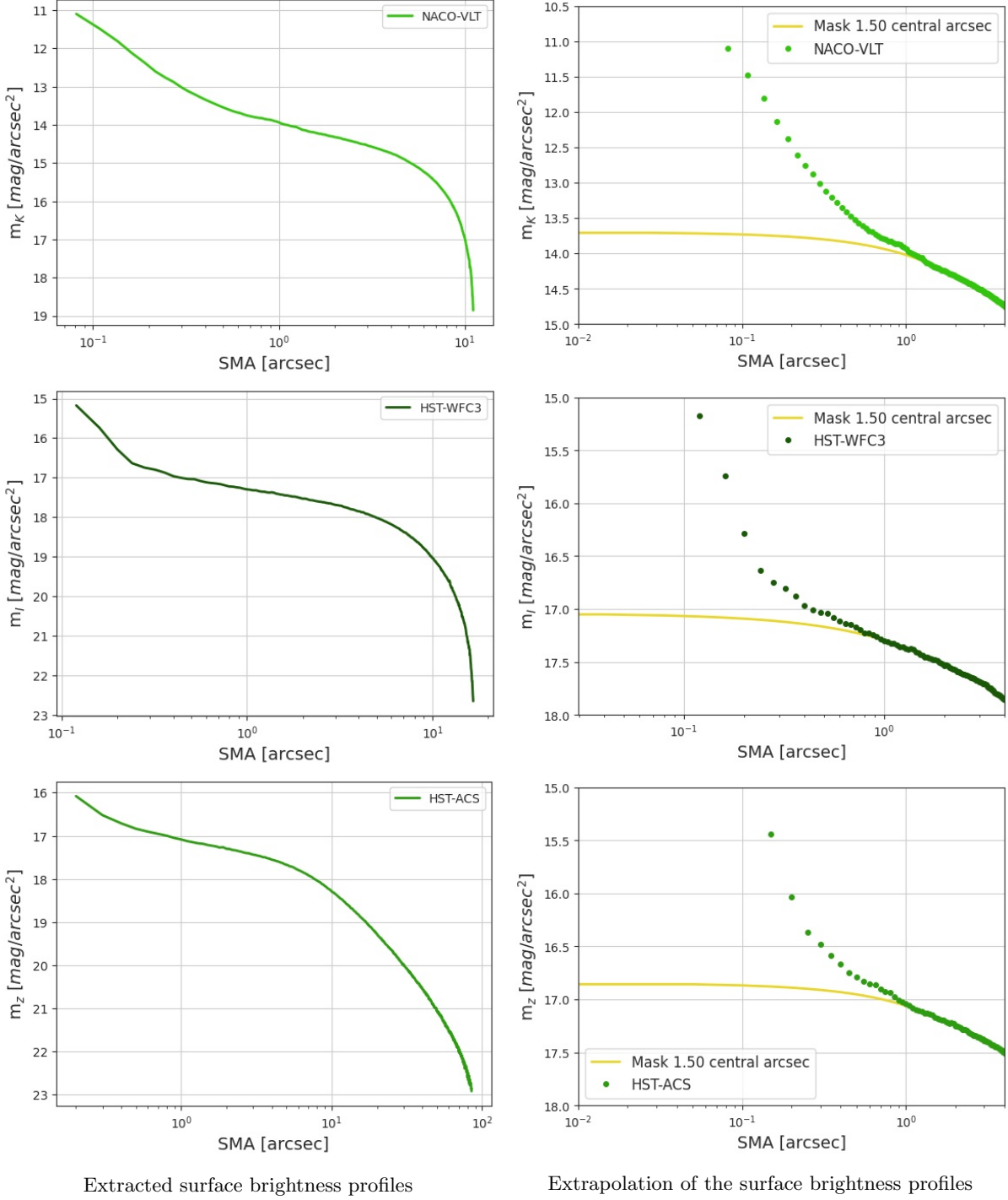


Figure 5: CCD image, model and residuals obtained for the NaCO-VLT and the HST-WFC3 images


 Figure 6: Surface brightness profiles extracted with the *ellipse* task and extrapolated.

M87 surface brightness is proved to follow a Sérsic profile, excluding the core region, but the actual values for its effective radius and the rest of Sérsic parameters are highly diverse and uncertain (Caon et al. 1990; De Vaucouleurs & Nieto 1978; Kormendy et al. 2009). Actually, the Sérsic profiles computed in the literature are studied in outer regions (from 15 to 420 " in Kormendy et al. (2009)) associated with the bulge of the galaxy, while our

profile is selected to study the most inner part of this bulge, in a region way closer to the nucleus ($< 85''$ for all of the observed images). Such nuclear profile does not precisely correspond to a Sérsic or any other deVaucouleurs distribution, and its parameters stop holding physical meaning when applied to such a smaller region.

For our work, instead of fitting or modeling the surface brightness profile to any preconceived profile function, we have decided to extrapolate the profile in the inner region in order to keep our data the most close possible to its real distribution while getting rid of the nucleus contribution. The distance chosen for starting the extrapolation is the closest one to $1.5''$ (approx 120 pc) away from the centre available in each extracted profile, selected from the HST-ACS profile where the data presents a inflexion point clearly detectable. The extrapolated profile follows the trend of the last points near the stopping point we are giving to the function. This happens due to the fact that when extrapolating we are not weighting the previous point from the further region.

D.2.3 Computation of the globular clusters subpopulations and radial distribution

In order to study the radial distribution of each GC subpopulations, first we needed to classify the globular clusters detected by Montes (2013) and Bellini et al. (2015) using their photometry data and its previously mentioned relation with the metallicity.

The GC distribution from Montes (2013), in the 38.4 inner acsec ($3 \times 3 \text{ kpc}^2$) of M87, present a mean colour of $V - I = 1.1$ mag, equivalent to a metallicity of $[\text{Fe}/\text{H}] = -0.75$ (see Figure 7). These values place most of this sample in the red subpopulation, according to the values derived by Kundu et al. (1999), that studied the M87 globular clusters subpopulation and their colour distribution. In order to obtain the number density of this sample of mainly red GCs, they were counted in four different radial bins of equal radii ($4.8''$), from 0 to $19''$ away from the center. The multiple radial bins and the globular clusters counted within each one can be seen in Table 1, and also the correspondent computed surface densities. Since the sample of GCs is formed of globular clusters detected in an observation image, the error associated with the GC counts was assumed to be Poissonian.

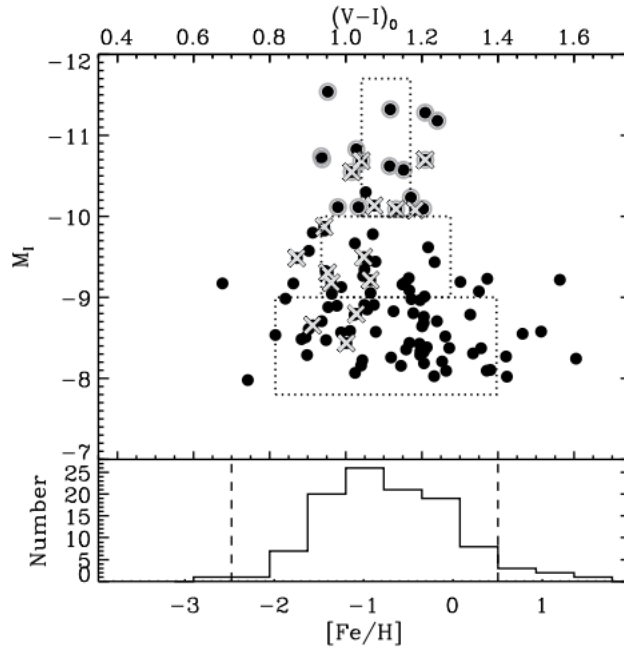


Figure 7: Histogram of V-I colour of the clusters from Montes (2013). The metallicity values indicated in the bottom x-axis were estimated using the linear transformation provided by Sohn et al. (2006). The dotted boxes represent magnitude intervals in y and the error of the median in x. Figure taken from Montes (2013)

Radial bin arcsec	n_{GC}	$N_{GC}\text{ arcsec}^{-2}$	$s(N_{GC})\text{ arcsec}^{-2}$
0 - 4.8	8	0.111	0.039
4.8 - 9.6	16	0.074	0.018
9.6 - 14.4	32	0.088	0.016
14.4 - 19.2	35	0.069	0.012

Table 1: Globular clusters counting and surface density. First column show the different considered radial bins, while the second columns present the counted GCs within each bin and the third column presents their correspondant number density.

A different procedure was follow for the Bellini et al. (2015) sample. By using the magnitudes obtained from the F606W and F814W HST filters, we have computed the colour $m_{F606W}-m_{F814W}$ (a good proxy for V - I) of the globular clusters. Based of the bimodality of the CMD diagram, presented in Figure 8, we decided to separate the two subpopulations by cutting in $m_{F606W}-m_{F814W} = 0.85$. This separation has implied a blue subpopulation of 735 globular clusters with a mean colour of $m_{F606W}-m_{F814W} = 0.754$ (with a standard deviation of 0.084), and a 1147 red one with $m_{F606W}-m_{F814W} = 0.985$ (with a standard deviation of 0.081). The GCs were counted in radial bins of 5'', from 0 to 80 '' (1.33'), and the associated errors were also considered to be Poissonian (check Table 2).

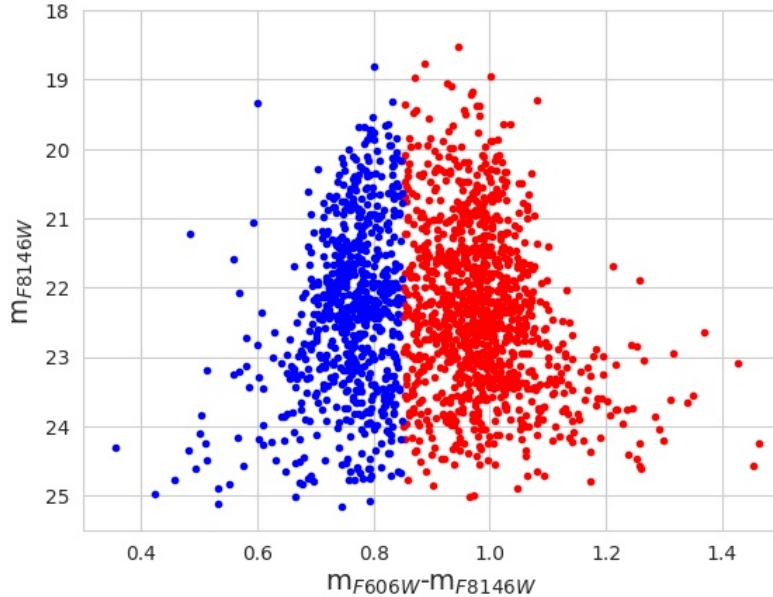


Figure 8: CMD of the globular clusters detected by Bellini et al. (2015). The colour bimodality of the sample divides it in the blue and red subpopulations, cutting at $m_{F606W}-m_{F814W} = 0.85$.

Radial bin	n_{GC}	N_{GC} arcsec $^{-2}$	$s(N_{GC})$ arcsec $^{-2}$	n_{red}	N_{red} arcsec $^{-2}$	$s(N_{red})$ arcsec $^{-2}$	n_{blue}	N_{blue} arcsec $^{-2}$	$s(N_{blue})$ arcsec $^{-2}$
arcsec									
0 - 5	10	0.127	0.040	9	0.115	0.038	1	0.013	0.013
5 - 10	16	0.068	0.017	11	0.047	0.014	5	0.0212	0.0095
10 - 15	36	0.092	0.015	23	0.059	0.012	13	0.0331	0.0092
15 - 20	49	0.089	0.013	26	0.0473	0.0093	23	0.0418	0.0087
20 - 25	61	0.086	0.011	46	0.0651	0.0096	15	0.0212	0.0055
25 - 30	62	0.0718	0.0091	46	0.0532	0.0079	16	0.0185	0.0046
30 - 35	89	0.0872	0.0092	50	0.0490	0.0069	39	0.0382	0.0061
35 - 40	80	0.0679	0.0076	50	0.0424	0.0060	30	0.0255	0.0046
40 - 45	93	0.0697	0.0072	68	0.0509	0.0062	25	0.0187	0.0037
45 - 50	105	0.0704	0.0069	65	0.0436	0.0054	40	0.0268	0.0042
50 - 55	103	0.0624	0.0062	68	0.0412	0.0050	35	0.0212	0.0036
55 - 60	97	0.0537	0.0055	62	0.0343	0.0044	35	0.0194	0.0033
60 - 65	104	0.0530	0.0052	64	0.0326	0.0041	40	0.0204	0.0032
65 - 70	100	0.0472	0.0047	63	0.0297	0.0037	37	0.0174	0.0029
70 - 75	118	0.0518	0.0048	73	0.0321	0.0038	45	0.0198	0.0029
75 - 80	91	0.0374	0.0039	56	0.0230	0.0031	35	0.0144	0.0024

Table 2: Globular clusters counting and surface density. First column show the different considered radial bins, while the second columns present the total counted GCs within each bin. The third column and fourth columns presents the total number density and their correspondant uncertainties. This structure is repeated for the next columns of the red and the blue subpopulation.

E Results and discussion

E.1 Surface brightness profiles

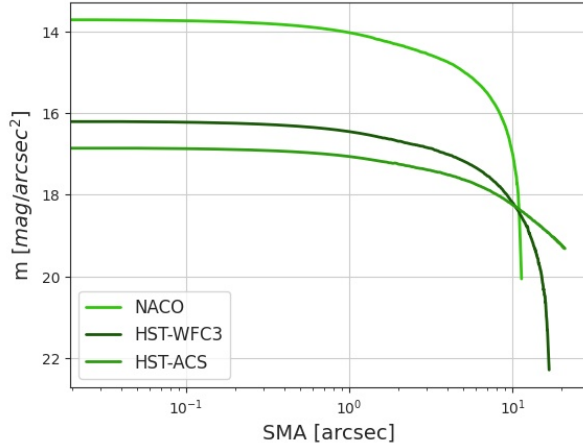


Figure 9: Extrapolated surface brightness profiles from the different images.

The M87 extracted and extrapolated surface brightness profiles (Section D.2.1 and Figures 3) are all presented and compared in Figure 6. The profiles extracted from the NACO-VLT and HST-WFC3 present a way more intense and rapid decrease for larger radial distances (actually semimajor axis lengths) than the HST-ACS profile, while previous studies show how M7 present a smooth behaviour in all bands (Montes 2013). This sharp behaviour does not agree with the expected behaviour for galaxy light distribution in the central region and neither matches previous results known for M87, such as Kormendy et al. (2009). The comparison between the surface brightness profile from Kormendy et al. (2009), also from HST-ACS WFC images, matches our extracted profile from HST-ACS WFC F850LP, as can be seen in Figure 7.

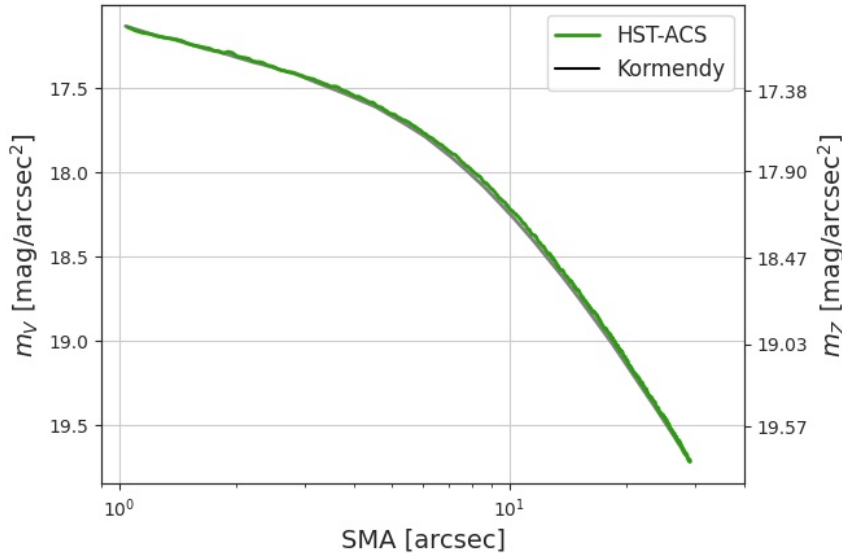


Figure 10: HST-ACS and Kormendy surface brightness profiles.

For the purpose of exploring the discordance in the NACO-VLT and HST-WFC3, we have compared the resulting surface brightness profiles with the correspondent line emission profile, selecting radial pixel lines from the center of M87. The compatibility between the extracted and the line profiles (see Figure 8) show an agreement with the data available within our images. After exploring different options, we have concluded that the reason behind this discordance could be due to the smaller field of view of both these images, or to some image border effects that can be affecting our data when extracting the profiles. This idea would also explain the fact that the NACO-VLT profile, with the smallest field of view, starts its decrease before the HST-WFC3 profile.

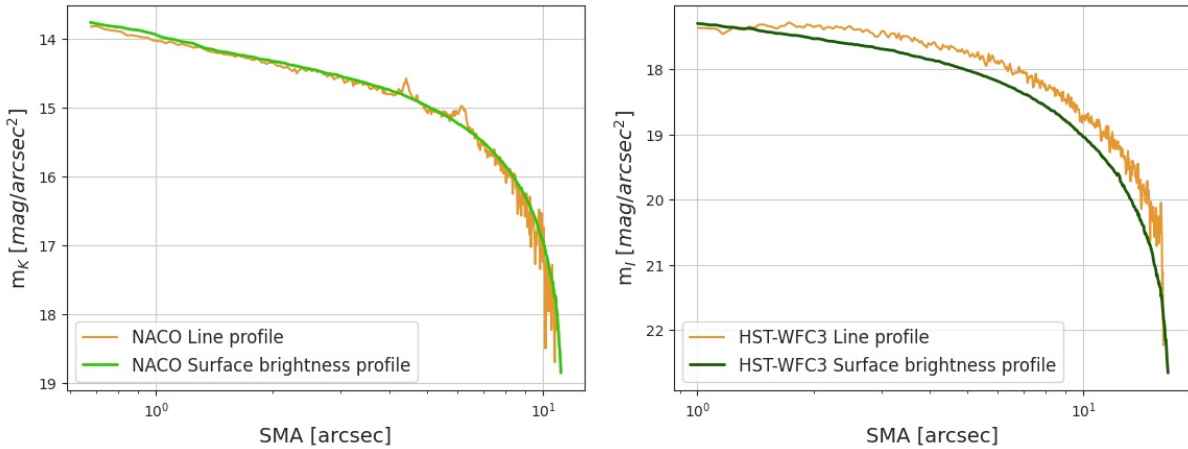


Figure 11: NACO-VLT and HST-WFC3 surface brightness and line profiles.

Taking all of this into account, we have decided to use the HST-ACS extrapolated profile, resolved till $85''$, for studying the relation between the light profile and the globular clusters radial distribution. Furthermore, the HST-ACS profile includes a wider field of view, which provides us more information in order to correctly reproduce the M87 bulge, while also keeping a good spatial resolution.

E.1.1 Globular cluster radial distribution

In Figure 12 (a), the GCs radial density distributions derived from the Montes (2013) and the Bellini et al. (2015) data are shown, along with the Sérsic profiles derived in Strader et al. (2011) are overplotted for comparison. For this comparison, we have calculated the number density for the whole GC population the Bellini et al. (2015) sample, using the same $0\text{--}19.2''$ binning as for the Montes (2013) data. The agreement between both samples in the inner region demonstrate the completeness of the Bellini et al. (2015) sample, that does not present any losses in GC detection, even though of observing in the optical-UV range (instead of infrared one), region where the dust might soften or disrupt the GCs contribution.

The computed GCs surface density, within the inner $1.33' \approx 80''$, present a flatter radial profile than the Strader et al. (2011) derived profiles. The different nuclear steep contribution modeled by Strader et al. (2011) is a result of the central extrapolation of their non-nuclear data (from $1'$ onwards), considering that GCs systems follow a Sérsic profile. In Figure 13 it can be seen how the radial number density for all the GCs (detected by Bellini et al. (2015)) is greater than the profiles extrapolated by Strader et al. (2011), even in the coincident regions (from $1'$ on). The greater amount of GCs within our sample are a consequence of the better spatial resolution and depth of the images involved in the detection processes.

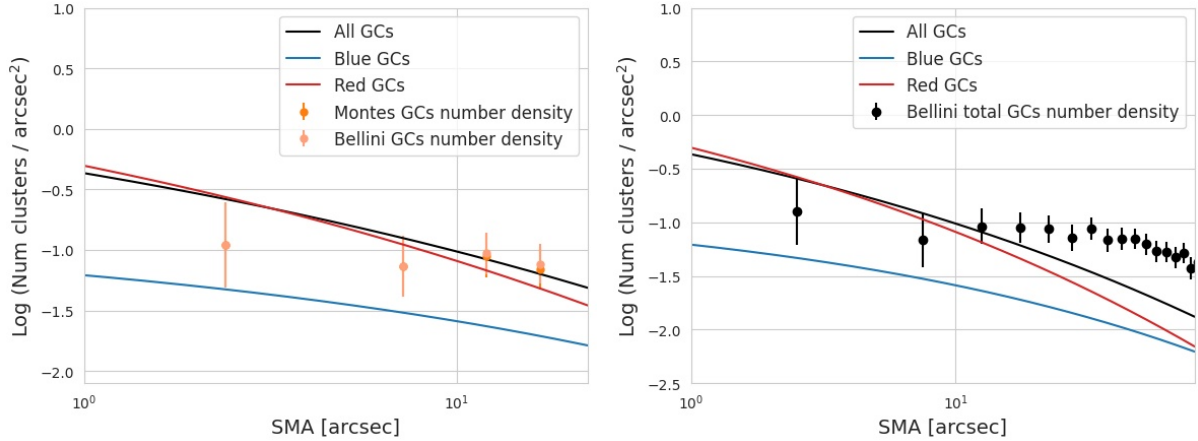


Figure 12: Globular cluster radial profiles

As in the Strader et al. (2011) profiles studied in outer regions, in Figure 13 it can be seen how the red GCs are also the main contribution to the total surface density of the whole population of globular clusters, in the central region. Accordingly, the blue system is less abundant and tends to decrease their presence towards the centre of M87, showing no overlap with the red subpopulation.

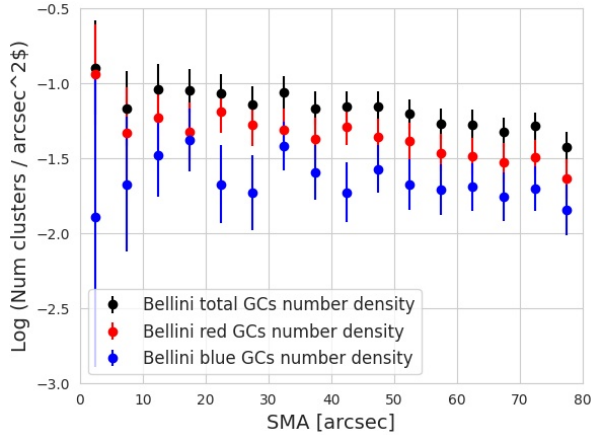


Figure 13: Globular cluster radial profiles

The comparison between the surface density profiles of each subpopulation and the M87 surface brightness profile can be seen in Figure 14. Since we are interested in the agreement between the shape of the profiles, we have decided to normalize both profiles (between their maximum and minimum values, including the associated uncertainties) for being able to establish a common reference frame. From around 35'' (2.7 kpc) away from the centre, both red and blue subpopulations show a similar decrease as the M87 light profile towards larger radii. Furthermore, red GCs even present the same trend till 20'' (1.5 kpc). Inside this radius, M87 presents a steeper increase than the red GCs profile. It is commonly found that, for giant elliptical galaxies and compact dwarfs (cD), the GC system density surface profile is generally flatter than the galaxy starlight (Bekki & Forbes 2006; Capuzzo-Dolcetta & Mastrobuono-Battisti 2009; Harris 1991). This difference can be due to GCs erosion, the missing GCs in the galactic central regions may have fed the central black hole, increasing the mass of the galactic centre. Observational support to this are the found correlations between the galaxy integrated absolute magnitude and the number of globular clusters lost and that between the central massive black hole mass and the total mass

of globular clusters lost (Capuzzo-Dolcetta & Mastrobuono-Battisti 2009).

Globular clusters from both subpopulations in the inner 20'', or even 35'', could have been dragged into the central black hole of M87, causing the observed drop of globular clusters surface density in these regions. But it must be taken into account that while the red globular clusters radial distribution presents a higher density and becomes flatter in these inner regions, the blue almost fades towards the centre. This difference for the red GCs and its higher surface density in the innermost regions must be taken into account along with other authors' results that show a match between the colour of the red subpopulation and M87 field stars. Tentatively, all these features together would support the scenario where red GCs were formed within M87, and some of the GCs within a few kpc of the galactic centre would have been dragged into the central black hole.

Since blue GCs⁷ radial distribution almost fades in the inner regions of M87 but is more extended at larger radii (Forbes et al. 2004; Harris 2009; Lauer & Kormendy 1986; Strader et al. 2011), along with the different metallicity, they can be tentatively considered to be formed in galaxies later canibalised by M87.

Another possible scenario that could explain the differences observed in the central profile for blue GCs and red GCs is based also in their metallicity difference. Both systems could have been formed within M87, and since blue GCs are metal-poor, they can be considered to be older than the metal-rich red GCs. Thus, the blue GCs would have been exposed longer to the gravitational potential of the M87 black hole, which would explain their lower presence in the BH nearest region. Yet, the main obstacles of these scenario would be the similar ages of both subpopulations, and also explaining their different surface density profiles in a galaxy-wide scale.

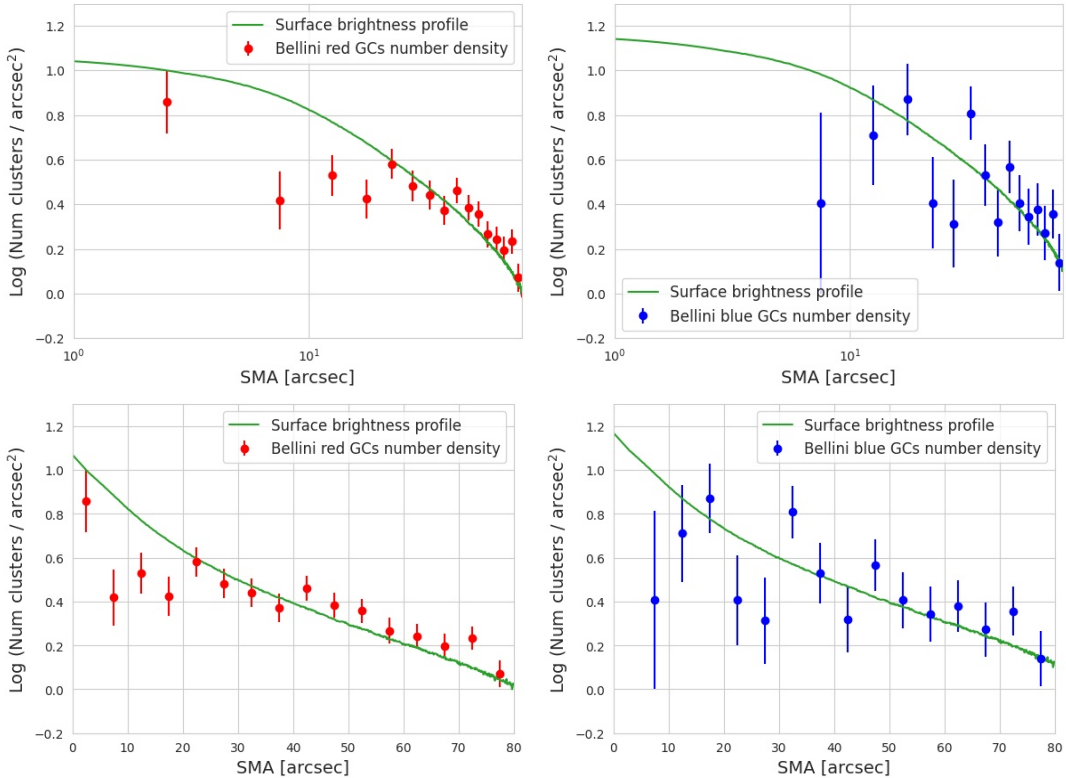


Figure 14: Globular cluster radial profiles

⁷It must be mentioned that the most central bin of the blue GCs density was not taken into account since the associated uncertainty is equal to the number density value.

F Conclusions

We have benefited from three previously observed M87 images of high spatial resolution for M87 in the near infrared and the infrared, taken with adaptive optics techniques using NaCO at VLT and the HST. This has permitted us to derive the M87 brightness profile in different bands, with an unprecedent spatial resolution (between 0.12 and 0.16 " due to the PSF of each observation). We have also benefited from the globular clusters detected by Montes (2013) and Bellini et al. (2015), that were also measured from AO images, in the infrared and the optical range, respectively. The high spatial resolution was essential to detect and accurately performed their photometry close to the nucleus of the M87 massive elliptical galaxy.

The main results of this project have been:

- The computation of the surface density profiles for the two GCs subpopulations, observed in the infrared, in the innermost region of 20 ". In addition, its agreement with the profiles derived from optical observations, till 1.33', that expose no dust extinction affecting the GCs detection.
- Red GCs keep dominating the GCs surface density profile in the inner region of $\pm 1.33'$. This result matches previous results obtained in wider distances, over 1'. The blue GCs surface density is slightly smaller than the red one for the whole studied region.
- After a radial distance of 35 " (2.7 kpc), both red and blue GCs present a decrease in their surface density towards greater radii that follows the same distribution as the M87 surface brightness profile. Furthermore, the red GCs keep following the M87 light profile trend till 20' (1.5 kpc). At his radius, the light profile of the galaxy drastically increases towards the centre, deviating even from the red GC distribution. These results, along with other authors' results could tentatively support the scenario where red GCs share a common formation scenario with M87, and some of the GCs within a few kpc of the galactic centre would have been dragged into the central black hole.

The main contribution of our work is the study of the GCs subpopulations in the innermost possible region of the galaxy, taking advantage of the highest available spatial resolution from AO instruments, and their relation with the M87 surface brightness profile. Further work of interest would be to derive the brightness profile of the globular clusters systems compare with the field stars surface brightness profile. This would allow us to establish a more consistent relation since we would be comparing the same physical property, the light distribution. Another work of interest would be to calculate the globular clusters mass percentage accreted by the central black hole (Capuzzo-Dolcetta & Mastrobuono-Battisti 2009).

References

- Bekki, K. & Forbes, D. A. 2006, *Astronomy & Astrophysics*, 445, 485
- Bellini, A., Renzini, A., Anderson, J., et al. 2015, *The Astrophysical Journal*, 805, 178
- Brodie, J. P. & Strader, J. 2006, arXiv preprint astro-ph/0602601
- Bruzual, G. & Charlot, S. 2003, *Monthly Notices of the Royal Astronomical Society*, 344, 1000
- Caon, N., Capaccioli, M., & Rampazzo, R. 1990, *Astronomy and Astrophysics Supplement Series*, 86, 429
- Capuzzo-Dolcetta, R. & Mastrobuono-Battisti, A. 2009, *Astronomy & Astrophysics*, 507, 183
- Cohen, J. G., Blakeslee, J. P., & Ryzhov, A. 1998, *The Astrophysical Journal*, 496, 808
- De Lucia, G. & Blaizot, J. 2007, *Monthly Notices of the Royal Astronomical Society*, 375, 2
- De Vaucouleurs, G. & Nieto, J.-L. 1978, *The Astrophysical Journal*, 220, 449
- Forbes, D. A., Brodie, J. P., & Grillmair, C. 1997, arXiv preprint astro-ph/9702146
- Forbes, D. A., Raul Faifer, F., Carlos Forte, J., et al. 2004, *Monthly Notices of the Royal Astronomical Society*, 355, 608
- Forte, J. C., Vega, E. I., & Faifer, F. 2012, *Monthly Notices of the Royal Astronomical Society*, 421, 635
- Harris, W. E. 1991, *Annual review of astronomy and astrophysics*, 29, 543
- Harris, W. E. 2009, *The Astrophysical Journal*, 703, 939
- Harris, W. E., Kavelaars, J., Hanes, D. A., Hesser, J. E., & Pritchett, C. J. 2000, *The Astrophysical Journal*, 533, 137
- Kormendy, J., Fisher, D. B., Cornell, M. E., & Bender, R. 2009, *The Astrophysical Journal Supplement Series*, 182, 216
- Kundu, A., Whitmore, B. C., Sparks, W. B., et al. 1999, *The Astrophysical Journal*, 513, 733
- Larsen, S. S., Brodie, J. P., Huchra, J. P., Forbes, D. A., & Grillmair, C. J. 2001, *The Astronomical Journal*, 121, 2974
- Lauer, T. R. & Kormendy, J. 1986, *The Astrophysical Journal*, 303, L1
- López-Navas, E. & Prieto, M. A. 2018, *Monthly Notices of the Royal Astronomical Society*, 480, 4099
- Montes, M. 2013, Ph. D. Thesis
- Peng, E. W., Jordán, A., Côté, P., et al. 2006, *The Astrophysical Journal*, 639, 95
- Sofue, Y. 1993, *Publications of the Astronomical Society of the Pacific*, 105, 308
- Sohn, S. T., O'connell, R. W., Kundu, A., et al. 2006, *The Astronomical Journal*, 131, 866
- Strader, J., Romanowsky, A. J., Brodie, J. P., et al. 2011, *The Astrophysical Journal Supplement Series*, 197, 33
- Vazdekis, A., Ricciardelli, E., Cenarro, A., et al. 2012, *Monthly Notices of the Royal Astronomical Society*, 424, 157

Appendix

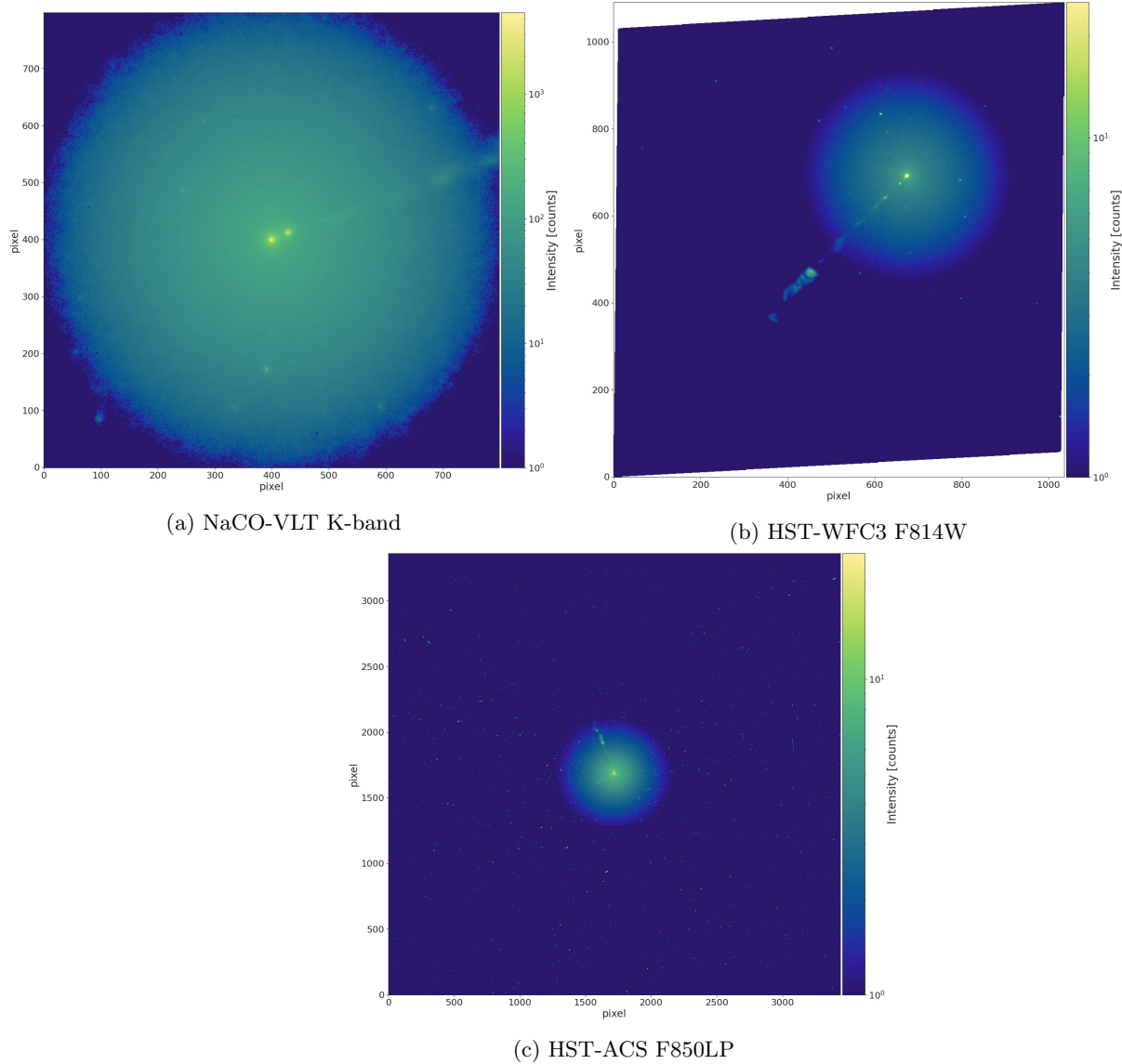


Figure A: CCD images studied in this work.